Desalination and Water Treatment
www.deswater.com

doi:10.5004/dwt.2019.23882

153 (2019) 145–156
June

GO/PDDA/Fe_3O_4 nanocomposites used for instaneous Cr(VI) removal and a reliable direct filtration-adsorption application

Xuezhen Feng[a], Yakun Zhang[a], Chunyan Liang[a], Jingang Yu[a,b], Xinyu Jiang[a,b,*]

[a]*School of Chemistry and Chemical Engineering, Central South University, Changsha 410083, China, email: fxz867545880@csu.edu.cn (X. Feng), zhangyk@csu.edu.cn (Y. Zhang), lcy7089@csu.edu.cn (C. Liang), yujg@csu.edu.cn (J. Yu), Tel. +86-0731-88879616, email: jiangxinyu@csu.edu.cn (X. Jiang)*
[b]*Key Laboratory of Hunan Province for Water Environment and Agriculture Product Safety, Changsha 410083, China*

Received 6 July 2018; Accepted 29 January 2019

ABSTRACT

A novel adsorbent, poly-(dimethyl diallyl ammonium chloride) (PDDA) functionalized graphene oxide (GO) further decorated with ferro ferric oxide (Fe_3O_4) nanoparticles, has been developed and used for instantaneous Cr(VI) removal from aqueous solution, and a reliable direct filtration-adsorption was achieved. Fourier transform infrared (FTIR) spectroscopy, Raman spectra (Raman), zeta potential measurement, scanning electron microscopy (SEM), high-resolution transmission electron microscopy (HRTEM), X-ray photoelectron spectroscopy (XPS) and differential pulse voltammetry (DPV) were adopted to confirm and investigate the chemical compositions, surface properties, morphological and electrochemical performance of the as-prepared magnetic nanocomposite (denoted as GO/PDDA/Fe_3O_4). The maximum adsorption capacity of GO/PDDA/Fe_3O_4 for Cr(VI) was 141.68 mg/g at pH = 2, and the desorption-regeneration results exhibited GO/PDDA/Fe_3O_4 could be a potential prospective nanocomposite used for instaneous filtration-adsorption of Cr(VI) from aqueous solution in real-life situations due to its fast, effective and stable properties.

Keywords: Water treatment; Cr(VI) removal; Adsorption; PDDA; Functionalized graphene oxide

1. Introduction

Hexavalent chromium [Cr(VI)] is one of heavy metals with strong oxidization and toxicity. It is difficult to degrade under natural conditions and easy to achieve toxic accumulation through the food chain, causing great harm to human beings and ecological environment. During recent years, a number of industrial applications of chrome are emerging. Meanwhile, being concerned with developing industries at a high speed, environmental protection is also an important aspect which needs to be considered. It is obvious that chrome-rich waste residues from chrome ore smelting, pigments, electroplating and other industrial productions need appropriate treatment to avoid indiscriminate discharge. And the researches on Cr(VI) removal technologies have always been proceeding.

In the traditional treatments, the reduction of Cr(VI) to Cr(III) and the precipitation of chromium hydroxide via addition of NaOH solution should be carried out due to the higher toxicity of Cr(VI) [1–3]. However, those methods possessed a few deficiencies, such as generated sludges, costly treatment equipment and reagents, inefficient recovery and so on [3,4]. Moreover, the conventional method could not apply to small-scale industries at all for lack of space. Many methods for the treatment of Cr(VI)-containing wastewater such as photocatalysis [5], capacitive deionization [6], adsorption [7] and so on have developed. Among them, adsorption could act as a more alternative technique for overcoming some above-mentioned limitations and possessing relatively better performance such as higher removal efficiency, less harmful emissions and the excellent recovery characteristics for adsorbed heavy metals [8,9].

As we all know, graphene oxide (GO) has already been applied in Cr(VI) removal due to its demonstrated good

*Corresponding author.

adsorption performance [10,11]. It contains sufficient oxygen-containing function groups, which makes itself more active and easier to modify. The surface of GO is negatively-charged, while Cr(VI) species exist in the form of negative acid ions ($Cr_2O_7^{2-}$, CrO_4^{2-} and $HCrO_4^-$). Novel GO-based materials, especially positively-charged GO composites with high affinity for anion, are expected to developed for achieving highly-efficient Cr(VI) removal from aqueous solution. For examples, Zhang et al. successfully synthesized polyaniline nanorods decorated GO nanosheets by dilute polymerization under –20°C as a novel super adsorbent for removal of Cr(VI), and it might be an excellent adsorbent due to superb removal capacity of 1149.4 mg/g for Cr(VI) [12]. The microwave preparation of triethylenetetramine modified GO/chitosan composite was also carried out, and the adsorbent could be easily recycled besides its excellent adsorption capacity for Cr(VI) [13].

Poly-(dimethyl diallyl ammonium chloride) (PDDA) is a strong cationic polyelectrolyte, which is soluble in water and possesses strong cohesion and good hydrolytic stability. In addition, it is insensitive to pH changes and presents chlorine resistance. PDDA was widely applied in the elimination of negative contaminants in aqueous solutions [14–16]. Moreover, the zeta-potential of PDDA/GO hybrid was found to be positive [17]. Therefore, PDDA could be proposed as a candidate for binding GO and employed in Cr(VI) removal.

Magnetic separation is regarded as a rapid and effective method for separating magnetic particles, which can be combined with adsorption [18,19]. By compositing with magnetite or iron ferrite, the obtained composite materials can be reinvested with ferromagnetism, and the separation procedure was then facilitated. For instance, Liu et al. [20] fabricated porous Fe_3O_4 hollow microspheres/GO composite for Cr(VI) removal; Jabeen et al. reported an enhanced Cr(VI) removal by iron nanoparticle decorated graphene [10]. Wang et al. investigated the synthesis of magnetic polypyrene decorated reduced GO-Fe_3O_4 composite and its application for the Cr(VI) removal [21]. Wang et al. fabricated core-shell magnetic Fe_3O_4@poly (m-phenylenediamine) particles for Cr(VI) reduction and adsorption [22]. Above researches indicated the practical application of magnetic carbon materials.

In this paper, PDDA functionalized GO (GO/PDDA) was synthesized by a simple mixing method, and then a facile reaction was exerted to decorate Fe_3O_4 nanoparticles onto GO/PDDA to obtain GO/PDDA/Fe_3O_4 nanocomposites (Fig. 1). Although GO/PDDA possessed good adsorption performance towards Cr(VI), it couldn't be easily separated from aqueous solutions. By coating with Fe_3O_4, both magnetic and membrane separation could be achieved and their adsorption capacity towards Cr(VI) increased. To investigate the adsorption capability of GO/PDDA/Fe_3O_4 nanocomposites for removal of Cr(VI) from water, the influences of initial Cr(VI) concentration, contact time, pH, co-existing ions and recycling number on the adsorption process were studied. The practical application of GO/PDDA/Fe_3O_4 nanocomposites for Cr(VI) by filtration-adsorption was further evaluated due to the instant adsorption equilibrium.

2. Materials and methods

2.1. Materials

Natural flake graphite (purity > 90%) was purchased from Shenzhen Nanotech Port Co., Ltd. PDDA was obtained from Aladdin Co. (1008 Qigang RD, Nanqiao Town, Fengx-

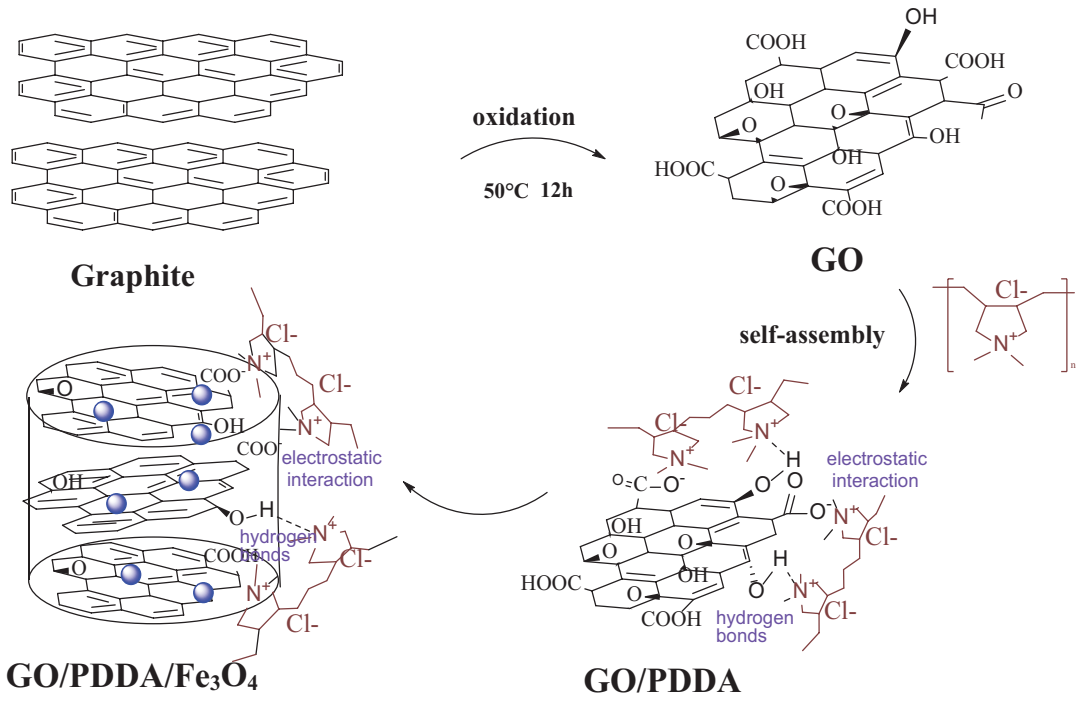

Fig. 1. The synthesis procedure of the GO/PDDA/Fe_3O_4 nanocomposites.

ian Shanghai,China). The Cr(VI) solutions were prepared by dissolving potassium dichromate ($K_2Cr_2O_7$) in deionized water. Potassium dichromate and ferrous chloride were obtained from Tianjin Fengchuan Chemical Reagent Technologies Co., Ltd. Ammonia solution (25%) and ferric chloride hexahydrate were bought from Kaixin Reagent Co., Ltd. and Sinopharm Chemical Reagent Co., Ltd., respectively. All chemicals were of analytical grade and used as received without any further treatment. Ultra-pure water was produced using a Milli-Q water purification system (Millipore, Milford, MA).

2.2. Fabrication of GO/PDDA/Fe_3O_4 nanocomposites

Preparation of GO:GO was synthesized by a modified Hummers method. Firstly, natural flake graphene (0.3 g) was evenly mixed with $KMnO_4$ (1.5 g) in a round-bottomed flask. And 40 mL of mixed acid including concentrated H_2SO_4 (36 mL) and H_3PO_4 (4 mL) was slowly dropped along the bottle wall into the reaction. Then, the mixture was stirred at 50°C in an oil bath for 12 h. Next, ice was added to dilute the suspension, and moderate amounts of H_2O_2 were added into the mixture until the diluted suspension became bright yellow. After that, the mixture was rinsed by HCl (1 mol/L) solution and ultra-pure water for 3–5 times. Finally, the obtained aqueous GO suspension was stored in a fridge at 4°C for future use.

Modification of GO with PDDA:Aqueous GO suspension was ultrasonically dispersed for 30 min before use. Then, GO dispersion (~5 mg/mL, 50 mL) was mixed with PDDA solution (25 mL), and the mixture was stirred for a few minutes. The GO/PDDA hydrogel was immersed in a large volume of ultrapure water to remove unattached PDDA. Finally, GO/PDDA was prepared by freeze-drying under vacuum for 24 h.

Synthesis of magnetic GO/PDDA/Fe_3O_4 nanocomposites: GO/PDDA (0.25 g) was dispersed in 100 mL of ultrapure water in a three-necked flask, then 0.5825 g of $FeCl_3{\cdot}6H_2O$ and 0.2408 g of $FeCl_2{\cdot}4H_2O$ were added under nitrogen atmosphere, and the mixture was mechanically stirred in an oil bath at 60°C. Ammonia solution (5 mL, 25%) was slowly added and the reaction was heated to 70°C under vigorous magnetic stirring for 4 h. Finally, GO/PDDA/Fe_3O_4 nanocomposites were separated from the solutions using a permanent magnet and rinsed with plenty of deionized water, and the product was freeze-dried, stored in an airtight container for further adsorption experiments. GO/Fe_3O_4 was prepared by the similar way for comparison.

2.3. Characterization of the samples

Fourier transform infrared (FTIR) spectra (Shimadzu FTIR spectrometer: model IR-prestige 21, Japan) and Raman spectroscopy (Renishamicro-Raman system 2000 spectrometer) were used to identify the introduced species. The specific surface areas of the samples were determined using a Kubo X1000 (Beijing, China) automatic physical absorber by the Brunauer–Emmett–Teller (BET) method. Scanning electron microscopy (SEM: JEOL, JSM-6360LV, Japan), together with a high-resolution transmission electron microscopy (HRTEM: JEOL, JEM-2100F, Japan; accelerating voltage 200 kV), were used to characterize the morphologies of the samples. The information concerning chemical compositions and formed bonds were obtained using an X-ray photoelectron spectroscopy (XPS: Perkin Elmer PHI 5000C ESCA instrument with Al Kα X-rays). Zeta potential analyzer (Zeta PALS 31510) measurement was applied to study the surface potentials for further explaining the adsorption mechanisms. Differential pulse voltammetry (DPV: CHI660E Electrochemical Workstation, Chenhua Instrument Co., Ltd. Shanghai, China) was employed to study the existing forms of chromium during the adsorption process.

2.4. Batch sorption experiments

Synthetized carbon nanocomposites (5 mg) were mixed evenly with Cr(VI) solution (20 mL) to obtain a turbid solution in an Erlenmeyer flask. Under oscillation (using a thermostat shaker), the adsorption process would occur and reach equilibrium. The initial and residual concentrations of Cr(VI) were evaluated by an inductive coupled plasma atom emission spectrometer (ICP-AES), and all turbid solutions containing solid and liquid phases after adsorption were filtered through 0.45 μm membranes (Shanghai Xinya Purification Materials Factory, Shanghai, China) before determination. The influences of contact time, initial Cr(VI) concentrations (10–60 mg/L, 10 mg/L intervals), pH values (2, 4, 6, 8, 10, 12), co-existing ions and recycle times were investigated. The Cr-loaded adsorbent was treated with 0.1 mol/L NaOH + 0.1 mol/L NaCl solution for 2 h [23,24] and separated by a magnet, and effects of adsorption/desorption times were also investigated. And the adsorption capacities were calculated using the following Eq. (1):

$$q_e = \frac{C_0 - C_e}{m} \times V \tag{1}$$

where q_e (mg/g) is the adsorption capacity of absorbent towards Cr(VI). C_0 and C_e (mg/L) are the initial and equilibrium concentrations of Cr(VI) solution, respectively. m (mg) is the mass of the absorbent, and V (L) is the Cr(VI) solution volume.

To further investigate the adsorption mechanism of GO/PDDA/Fe_3O_4 for Cr(VI), adsorption kinetics were fitted by pseudo-first-order, pseudo-second-order, Elovich equation and intraparticle diffusion models [25–28] in this study. And the four equations are expressed as follows:

Pseudo-first-order equation: $$\log(q_e - q_t) = \log q_e - \frac{k_1}{2.303} t \tag{2}$$

Pseudo-second-order equation: $$\frac{t}{q_t} = \frac{1}{k_2 q_e^2} + \frac{1}{q_e} t \tag{3}$$

Elovich equation: $$q_t = \frac{1}{\beta}\ln(\alpha\beta) + \frac{1}{\beta}\ln t \tag{4}$$

Intraparticle diffusion kinetic model: $$q_t = K_p t^{1/2} + C \tag{5}$$

where q_e (mg/g) and q_t (mg/g) refer to the amount of Cr(VI) ions adsorbed by the GO/PDDA/Fe_3O_4 at equilibrium and at time t (min), respectively; k_1 (min^{-1}) and k_2 (g $mg^{-1}min^{-1}$) [Eqs. (2), (3)] represent the rate constant of the pseudo-first-order kinetic adsorption and the pseudo-second-order kinetic

adsorption, respectively; α (g/(mg min) is the original adsorption rate and β (g/mg) is the desorption constant in connection with the extent of surface coverage and activation energy constant for chemisorption (Eq. (4)); k_p (mg/(g min)) is the diffusion rate constant, and constant C is associated with thickness of the boundary layer [Eq. (5)].

2.5. Filtration-adsorption and desorption experiments

Membranes (0.45 μm, Shanghai Xinya Purification Materials Factory, Shanghai, China) were decorated by GO/PDDA/Fe_3O_4 for filtration-adsorption experiments. Firstly, a certain amount of synthetized GO/PDDA/Fe_3O_4 was mixed evenly with ultrapure water to obtain a turbid solution, and then suction filtration was employed to remove water and make sure that GO/PDDA/Fe_3O_4 evenly coated the membrane. The dosage of GO/PDDA/Fe_3O_4 determined the thickness, which mattered a lot to the adsorption. A certain amount (5 mg, 10 mg) of synthetized GO/PDDA/Fe_3O_4 was chosen to investigate the influences of Cr(VI) solution concentrations (10–60 mg/L, 10 mg/L intervals). And 0.1 mol/L NaOH + 0.1 mol/L NaCl solution was employed in filtration-desorption.

3. Results and discussion

3.1. Characterization of samples

Fig. 2a shows FT-IR spectra of GO, Fe_3O_4, GO/Fe_3O_4, GO/PDDA and GO/PDDA/Fe_3O_4, respectively. FT-IR spectra of GO presents the characteristic peaks of oxygen-containing groups such as carboxyl groups (C=O) at 1738 cm^{-1}, hydroxyl species at 1420 cm^{-1} and 1227 cm^{-1} (O-H stretching and deformation vibrations) and epoxy species at 1056 cm^{-1} and 849 cm^{-1} (C-O-C stretching vibration) [29]. As can be seen in FT-IR spectra of GO-based composites, the broad peak at around 3422 cm^{-1} could be attributed to the O-H stretching vibration of the carboxylic acids groups and the peaks located at 1626 cm^{-1} belongs to C=O stretching vibration. As for the FT-IR spectra of GO/PDDA and GO/PDDA/Fe_3O_4, the emerging peak at 2935 cm^{-1} belongs to the C-H stretching vibration of -CH_3 of PDDA [30], and the characteristic peak at 1470 cm^{-1} could be attributed to the C-N stretching vibration of polyquaternary amine. And the peaks between 1240 and 945 cm^{-1} due to N-H bending vibrations could be found [31,32]. The coated PDDA was confirmed by FT-IR spectroscopy. In addition, the peak at 576 cm^{-1} of GO/PDDA/Fe_3O_4 provides strong evidence for the presence of Fe-O bond vibration. In conclusion, PDDA and Fe_3O_4 were successfully incorporated with GO.

Raman spectroscopy was employed to evaluate the disorder and defects on the GO-based samples (Fig. 2b).The obvious peaks at 1326 (*D* band) and 1582 cm^{-1} (*G* band) can be attributed to the disordered structure of sp^3 carbon atoms and the graphite structure of sp^2 carbon atoms in graphitic sheets of GO, respectively [33–35]. Compared to GO, the absorption bands of other three materials are relatively well-kept, and the peaks at 222 cm^{-1} and 280 cm^{-1} belong to Fe_3O_4, whereas the redshifted G bands of GO/PDDA/Fe_3O_4 and GO/Fe_3O_4 could also be observed, indicating the existing strong interactions between GO and Fe_3O_4. In comparison with pristine GO with an integrated intensity ratio (I_D/I_G) of 1.124, the I_D/I_G of GO/Fe_3O_4, GO/PDDA and GO/PDDA/Fe_3O_4 were 1.292, 1.229 and 1.427, respectively, indi-

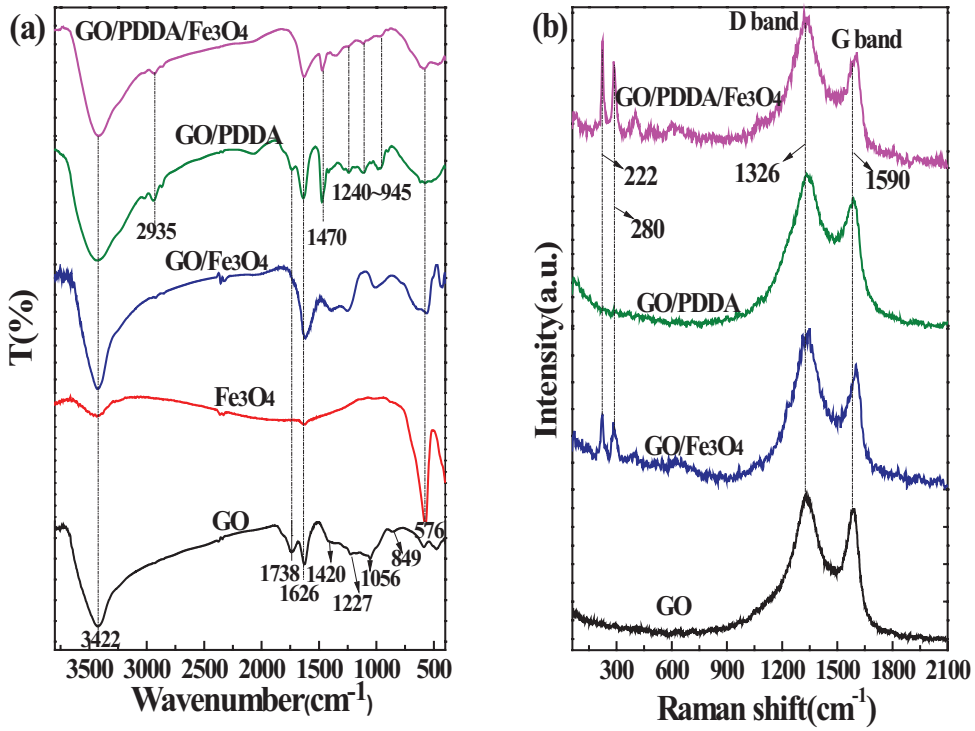

Fig. 2. (a) The FT-IR spectra of GO, Fe_3O_4, GO/Fe_3O_4, GO/PDDA and GO/PDDA/Fe_3O_4; (b) Raman spectra of GO, GO/Fe_3O_4, GO/PDDA and GO/PDDA/Fe_3O_4.

cating higher disorders could be observed for the functionalized samples [36].

Fig. 3 shows representative N_2 adsorption-desorption isotherms and the corresponding BJH pore distribution (built-in) of GO/PDDA/Fe_3O_4. The isotherms belonged to a typical type IV isotherm. According to the Brunauer-Emmett-Teller (BET) method, the calculated specific surface area of GO/PDDA/Fe_3O_4 is 7.84 m^2/g. The pore size distribution calculated by BJH methods demonstrated the existence of massive mesopores in GO/PDDA/Fe_3O_4 with average sizes of ~7.44 nm.

The electrostatic potentials of GO modified with PDDA and Fe_3O_4 were investigated by zeta-potential measurement (Fig. 4). The concentrations of samples were 1 mg/mL. Zeta potentials were converted to negative with an increased pH, then the adsorption capacity of GO/PDDA/Fe_3O_4 for anionic dichromate ions reduced. GO was usually negatively charged, while PDDA was a cationic polyelectrolyte agent. It was obvious that the mean zeta-potentials of GO/PDDA and GO/PDDA/Fe_3O_4 were still positive (4.24~47.25 mV) in water due to the introduced PDDA, which was beneficial to the adsorption for anionic dichromate ions [16,17].

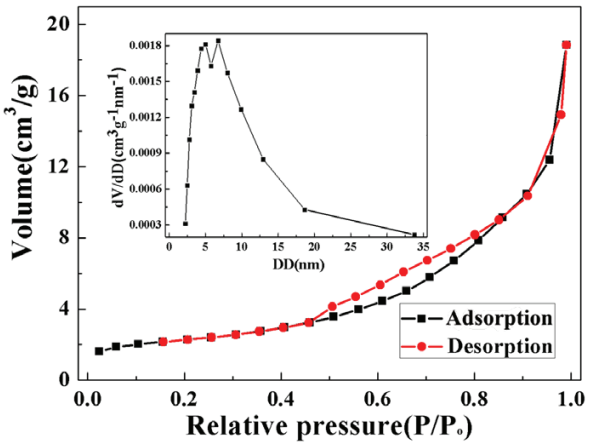

Fig. 3. N_2 adsorption-desorption isotherm and (inset) BJH pore distribution of GO/PDDA/Fe_3O_4.

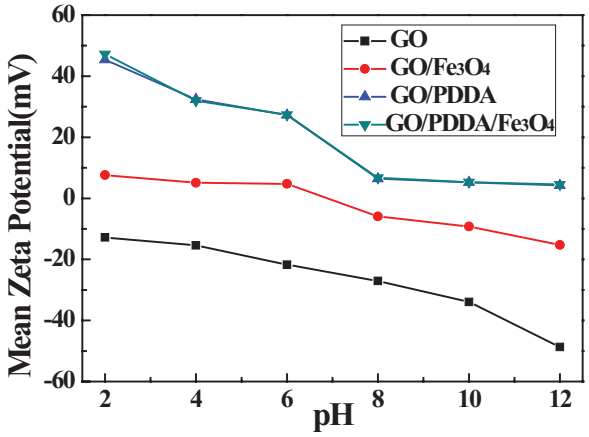

Fig. 4. The zeta-potential measurement of the GO, GO/Fe_3O_4, GO/PDDA and GO/PDDA/Fe_3O_4 at different pH values.

XPS spectra analysis of GO/PDDA/Fe_3O_4 was performed to discover the decoration and existing forms of Fe_3O_4 and PDDA on the surface of GO (Fig. 5). The peaks of N1s (402.06 eV) and Fe2p (710.77 eV) are clearly obvious in survey spectra (Fig. 5a); and the N1s scan data indicated the existing of quaternary ammonium (402.06 eV) of PDDA. Simultaneously, the Fe2p envelope contains two peaks at 710.7 and 724.6 eV (Fig. 4b) which could be assigned to $Fe2p_{3/2}$ and $Fe2p_{1/2}$, respectively. From the XPS analysis, it is obvious that the GO was successfully functionalized with Fe_3O_4 and PDDA.

Field emission scanning electron microscopy (FE-SEM) and transmission electron microscopy (TEM) was used to illustrate the morphologies of the materials. As it can be seen in the SEM images (Figs. 6a–d), two-dimensional lamellar structure of GO is obvious, and its surfaces are very flat and smooth, while PDDA functionalized GO is wrinkle and thickened (Fig. 6a). GO/PDDA is a little fuzzy with curling edges, and it's obvious that aggregation occurred (Fig. 6b). When composited with Fe_3O_4, the introduced Fe_3O_4 nanoparticles would be distributed sporadically in the GO/Fe_3O_4 (Fig. 6c) or GO/PDDA/Fe_3O_4 (Fig. 6d), and GO nanosheets were also damaged to a certain extent in the modification process. Additionally, the grafting of PDDA weakened the destruction towards the carbon structure. TEM images of GO/PDDA and GO/PDDA/Fe_3O_4 were shown in Fig. 6e and Fig. 6f, respectively. The emerging clew-like nanostructures with lateral dimension of 0.25 micrometers represented the introduced PDDA. From TEM image of GO/PDDA/Fe_3O_4, it could be seen that Fe_3O_4 with particle sizes of 3–5 nm were well deposited on the surface of GO (Fig. 6f).

3.2. Effects of condition parameters on the adsorption of Cr(VI)

Batch adsorption experiments using GO/Fe_3O_4, GO/PDDA and GO/PDDA/Fe_3O_4 for dichromate ions ($Cr_2O_7^{2-}$) solutions with different initial concentrations were conducted (Fig. 7a). It should be pointed out that with the versatility of PDDA and Fe_3O_4, and magnetic separation could be achieved by using GO/PDDA/Fe_3O_4 as the adsorbent (Fig. 7b). In addition, GO/PDDA/Fe_3O_4 possessed the highest adsorption capacity (approximately 100 mg/g), which was higher than those of GO/Fe_3O_4 (~4 mg/g) and GO/PDDA (~70 mg/g). As depicted in Fig. 8, the adsorption process was near instantaneous and the adsorption equilibrium was reached in a few seconds.

The adsorption capacities of as-prepared GO/PDDA/Fe_3O_4 for Cr(VI) at different pH values are shown in Fig. 9. The adsorption capacities increased with the decrease of pH values of $Cr_2O_7^{2-}$ solutions, indicating the competitive adsorption between hydroxyl ions and $Cr_2O_7^{2-}$ under alkaline conditions (as shown in Eqns. (6)–(9), where R represents the aliphatic groups):

$$R_4\text{-}N^+ + Cr_2O_7^{2-} \rightleftharpoons R_4\text{-}N^{+}\cdots Cr_2O_7^{2-} \quad (6)$$

$$Cr_2O_7^{2-} + 2OH^- \rightleftharpoons 2CrO_4^{2-} + H_2O \quad (7)$$

$$R_4\text{-}N^+ + CrO_4^{2-} \rightleftharpoons R_4\text{-}N^{+}\cdots CrO_4^{2-} \quad (8)$$

$$R_4\text{-}N^+ + OH^- \rightleftharpoons R_4\text{-}N^{+}\cdots OH^- \quad (9)$$

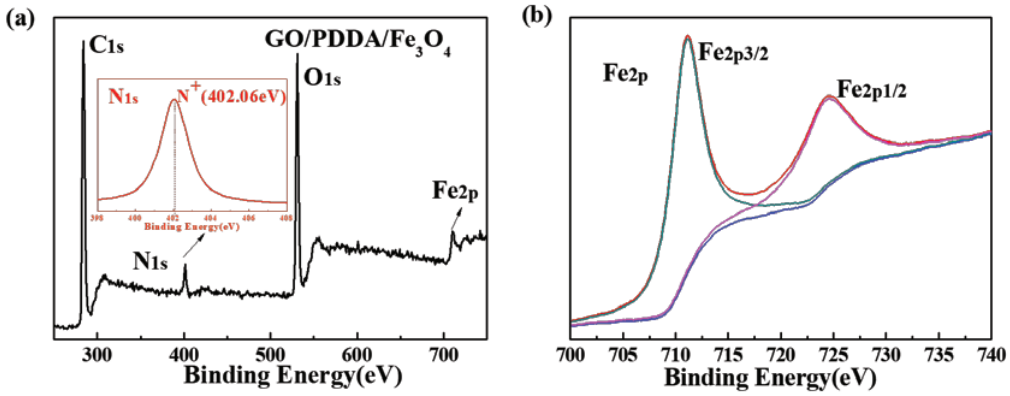

Fig. 5. XPS spectra analysis of GO/PDDA/Fe_3O_4: (a) survey spectra of XPS data; (b) higher resolution of Fe2p XPS spectra.

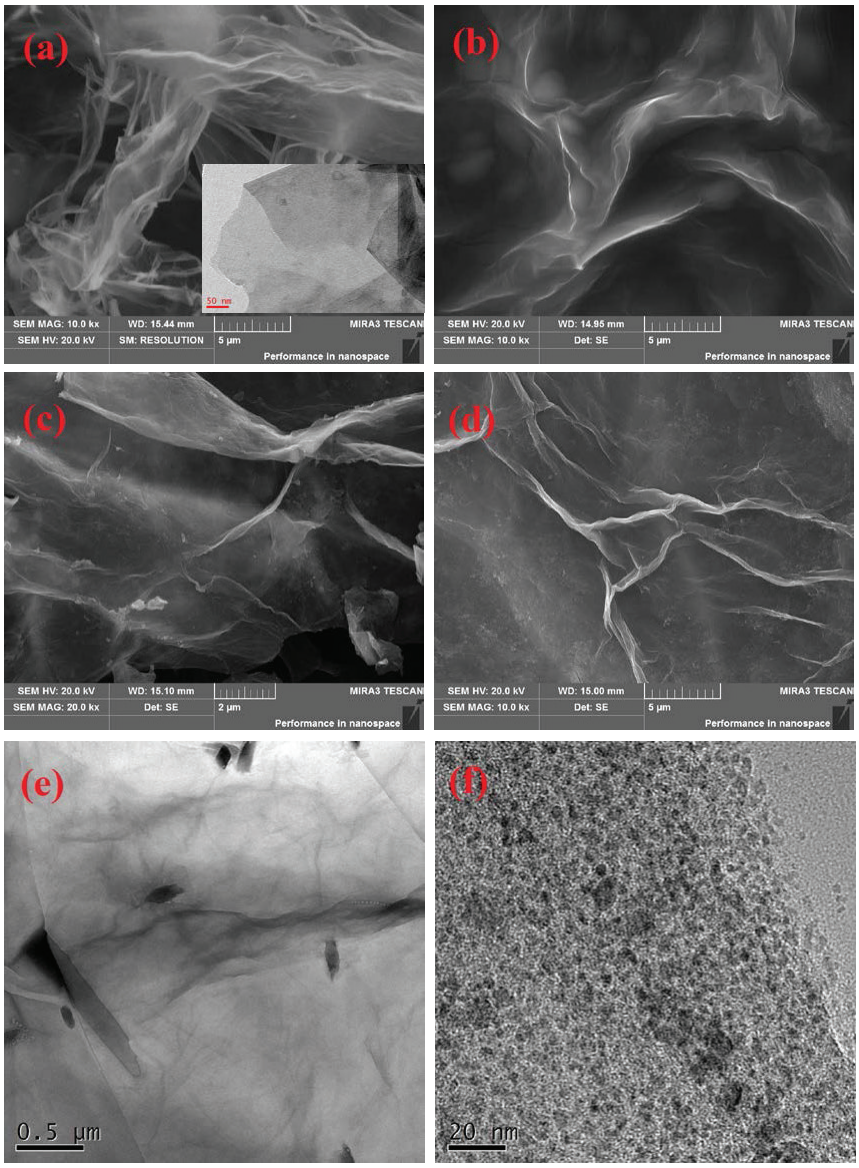

Fig. 6. SEM images of GO (a), GO/PDDA (b), GO/Fe_3O_4 (c), and GO/PDDA/Fe_3O_4 (d); TEM images of GO (a), inline image in the lower right corner), GO/PDDA (e), GO/PDDA/Fe_3O_4 (f).

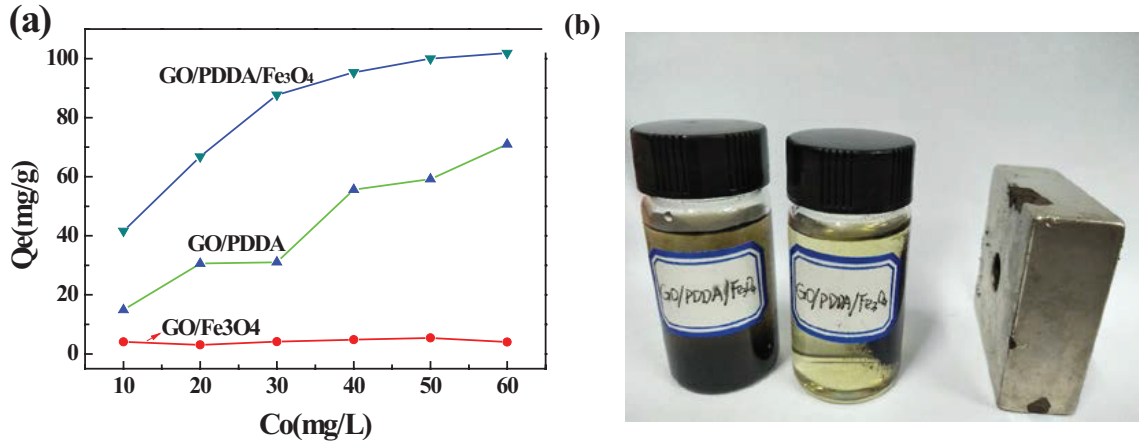

Fig. 7. (a) Adsorption capacities of different materials towards different Cr(VI) ionic strength; (b) Photograph demonstrating the separation of GO/PDDA/Fe_3O_4 from solution using a magnet.

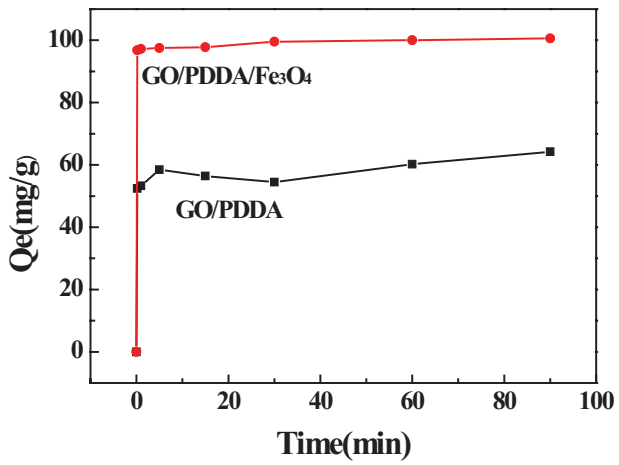

Fig. 8. Effect of contact time on the adsorption of Cr(VI) ($C_{Cr(VI)}$ = 50 mg/L) by GO/PDDA/Fe_3O_4.

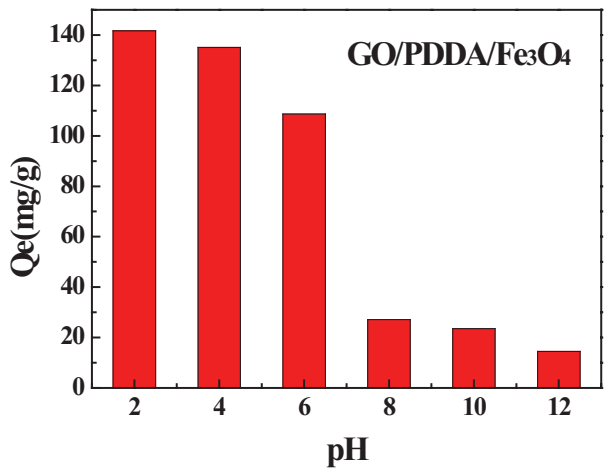

Fig. 9. Effect of solution pH on the adsorption of Cr(VI) ($C_{Cr(VI)}$ = 50 mg/L) by GO/PDDA/Fe_3O_4.

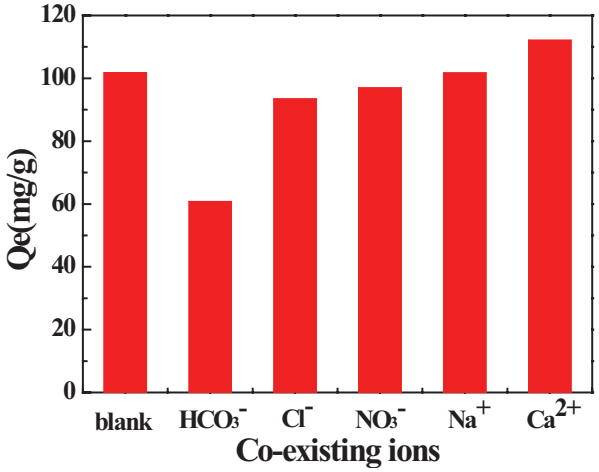

Fig. 10. Effects of co-existing ions in underground water on the adsorption of Cr(VI) ($C_{Cr(VI)}$ = 50 mg/L) by GO/PDDA/Fe_3O_4.

And acidic pH values were beneficial to the adsorption process. Actually, H_2CrO_4, $HCrO_4^-$, CrO_4^{2-} and $Cr_2O_7^{2-}$ were the dominating Cr(VI) species [37,38]. On the one hand, the reduction of Cr(VI) to Cr(III) took place and surface-modified Fe_3O_4 nanoparticles could form coordination bonds with Cr(III) [39,40], which was expatiated in the adsorption mechanism. On the other hand, electrostatically induced aggregation of quaternary amine chains of PDDA was partly loosed under acidic condition, which promoted the electrostatic attraction between GO/PDDA/Fe_3O_4 and Cr(VI).

With regard to the influence of co-existing ions in environmental water samples, the effects of some co-existing metal ions were also investigated (Fig. 10). Those co-existing metal ions, except for bicarbonate ions, exhibited relatively moderate effects on the removal efficiencies of GO/PDDA/Fe_3O_4 for Cr(VI). The observed phenomenon suggested that there was electrostatic adherence between dichromate ions ($Cr_2O_7^{2-}$) and GO/PDDA/Fe_3O_4. Therefore, GO/PDDA/Fe_3O_4 could be practically used in the treatment of wastewater containing dichromate ions ($Cr_2O_7^{2-}$).

3.3. Adsorption kinetics

The adsorption rate of GO/PDDA/Fe_3O_4 towards Cr(VI) was investigated through four kinetics models (i.e., pseudo-first-order, pseudo-second-order, Elovich and intraparticle diffusion models), which could be used to investigate whether the process was controlled by chemical or physical adsorption. The kinetic parameters for the adsorption of Cr(VI) onto GO/PDDA/Fe_3O_4 at room temperature at pH = 2 of the four models were listed in Table 1 and the corresponding isotherms are listed in Fig. 11. The pseudo-second-order kinetic model better fitted the data (R^2 > 0.999) than other three kinetic models, where the calculated q_e (100.6 mg/g) was in agreement with the real experimental result (approximately 100 mg/g), indicating that chemisorption was the rate-controlling step in the adsorption process [41].

Table 1
Kinetic parameters for the adsorption of Cr(VI) onto GO/PDDA/Fe_3O_4 at room temperature at pH = 2

Model	Parameter	Parameter value
Pseudo-first-order	q_e (mg/g)	3.652
	k_1 (min^{-1})	0.07140
	R^2	0.9313
Pseudo-second-order	q_e (mg/g)	100.6
	K_2 (g/(mg min))	0.05399
	R^2	0.9999
Elovich model	α (mg/(mg min))	$1.3*10^{69}$
	β (g/mg)	1.642
	R^2	0.7760
Intraparticle diffusion models	K_p (mg/g min)	0.4316
	R^2	0.9418

3.4. Desorption and regeneration study

In consideration of practical application, absorbents cyclic utilization is part and parcel of stress, where it is weighed that the cost of the materials production against the benefits it will bring. Combined with the discussion above, the pH-dependent adsorption preferred acidity and the desorption of the dichromate ions ($Cr_2O_7^{2-}$) could be achieved through an alkaline condition. Therefore, 0.1 mol/L NaOH solutions were used for recycling and regeneration of the absorbent. The FT-IR spectra of GO/PDDA/Fe_3O_4, GO/PDDA/$Fe_3O_{4Cr\text{-}loaded}$, GO/PDDA/$Fe_3O_{4desorption}$ are demonstrated in Fig. 12a, the basic functional groups were preserved well whether adsorption or desorption, and the peaks at 753 cm^{-1} (Cr-O) and 944 cm^{-1} (Cr=O) from chromium were visible. Meanwhile, as demonstrated (Fig. 12b), undergoing five cycles, only a slight decrease emerged and GO/PDDA/Fe_3O_4 possessed a stable adsorption capacity (~84 mg/g), which was a direct reflection of cyclic utilization achievement.

3.5. Adsorption mechanism analysis

As shown in Fig. 13, positively charged GO/PDDA/Fe_3O_4 could adsorb negatively charged dichromate ions

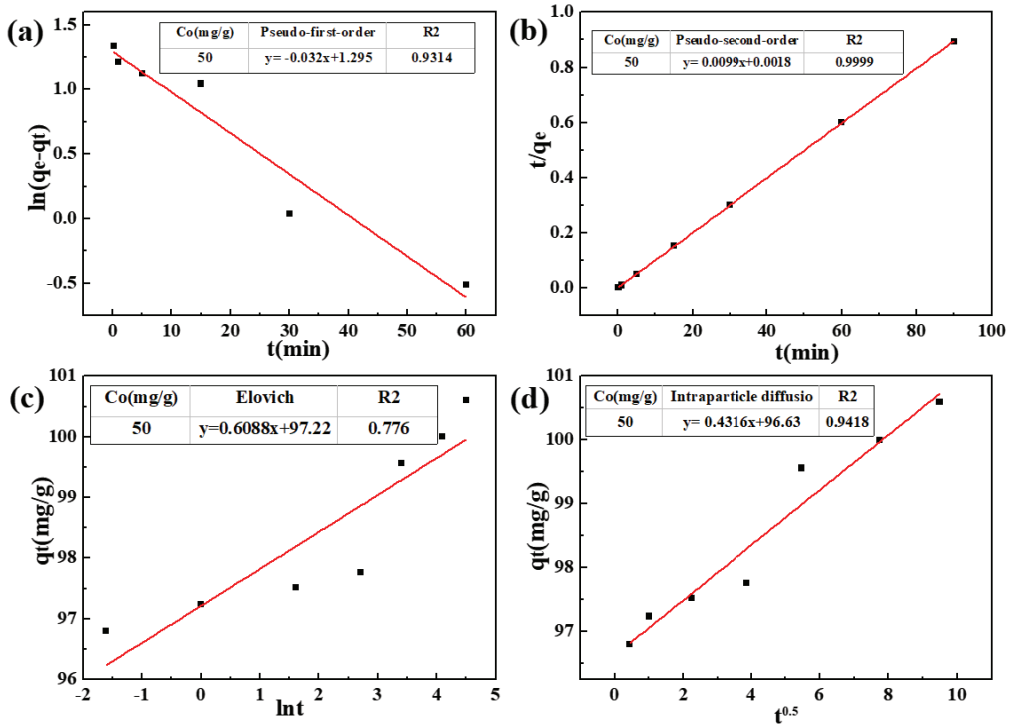

Fig. 11. Four linear kinetic models of Cr(VI) adsorption ($C_{Cr(VI)}$ = 50 mg/L) by GO/PDDA/Fe_3O_4: (a) Pseudo-first-order; (b) Pseudo-second-order; (c) Elovich; (d) Intraparticle diffusion.

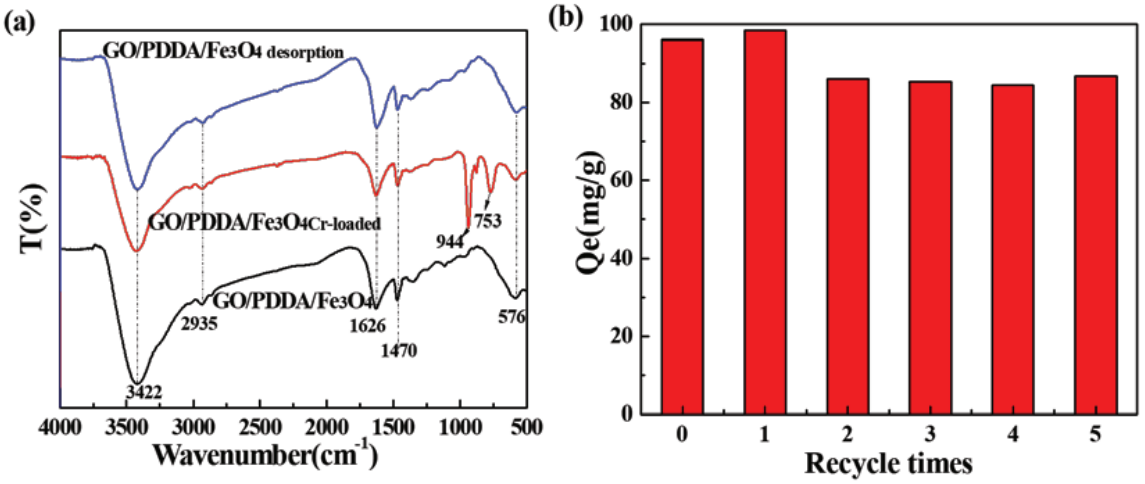

Fig. 12. (a) The FT-IR spectra of GO/PDDA/Fe_3O_4, GO/PDDA/$Fe_3O_{4\ Cr\text{-}loaded}$, GO/PDDA/$Fe_3O_{4\ desorption}$; (b) Reusability of GO/PDDA/Fe_3O_4 for Cr(VI) ($C_{Cr(VI)}$ = 50 mg/L) adsorption.

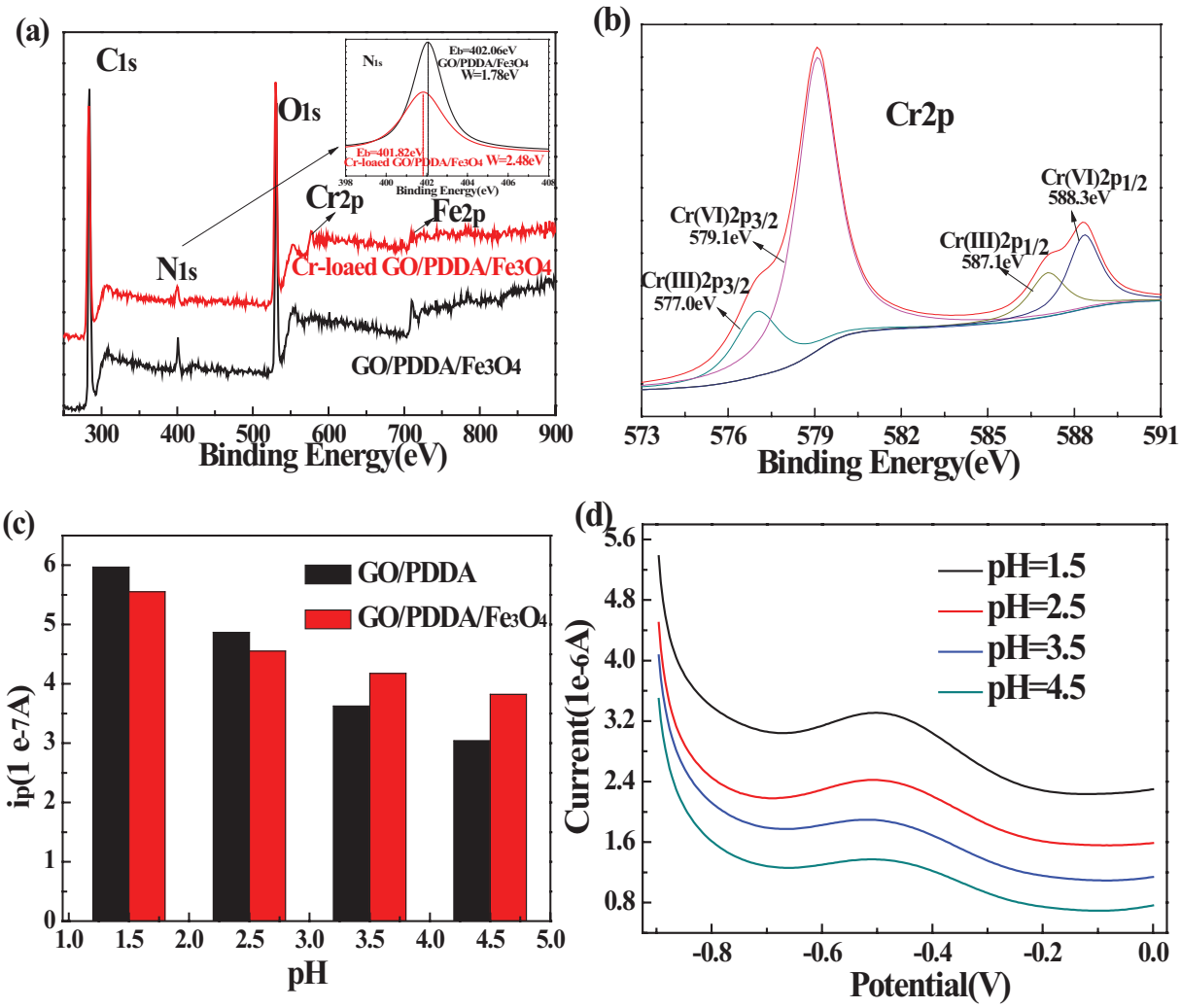

Fig. 13. (a) XPS spectra analysis of GO/PDDA/Fe_3O_4 and GO/PDDA; (b) higher resolution of Cr2p XPS spectra; (c) Response currents for decreasing pH of Cr(VI) (50 mg/L) at a scan rate 50 mV/s and in the presence of GO/PDDA/ Fe_3O_4 and GO/PDDA (1.0 mg/mL); (d) DPV for decreasing pH of Cr(VI) (50 mg/L) at a scan rate 50 mV/s and in the presence of GO/PDDA/ Fe_3O_4 (1.0 mg/mL).

($Cr_2O_7^{2-}$) through strong electrostatic attraction. Another reason for the higher adsorption capacity of GO/PDDA/Fe_3O_4 towards Cr(VI) could be the reduction of Cr(VI) to Cr(III) and the reactions are shown as Eqs. (10), (11) [42], and the Cr(III) species could be adsorbed through the complexation with the oxygen-containing functional groups of GO/PDDA/Fe_3O_4.

$$HCrO_4^- + 7H^+ + 3e^- \rightleftharpoons Cr^{3+} + 4H_2O \quad (10)$$

$$Cr_2O_7^{2-} + 14H^+ + 6e^- \rightleftharpoons 2Cr^{3+} + 7H_2O \quad (11)$$

To further dive deep into the adsorption mechanism of Cr(VI) on GO/PDDA/Fe_3O_4, XPS (Figs. 13a–d) was employed there. The XPS (Fig. 13a) of GO/PDDA/Fe_3O_4 and Cr-loaded GO/PDDA/Fe_3O_4 offered the contrast, where the new peaks of Cr2p and a found trifling shifted to lower binding energy of N1s (Fig.11a-embedded diagram) after adsorption briefly showed the adsorbed Cr. On the one hand, the binding energy at 402.06 eV could be assigned to the nitrogen atoms in the N^+ groups and the adsorption towards Cr resulted in the shift to neutral binding energy at 401.82 eV [43]. And the largest discrepancy was the half-peak width, which made explanations that the amine groups were the active involvement in the Cr(VI) uptake. On the other hand, the exists of both Cr(VI) and Cr(III) shown in higher resolution of Cr2p XPS spectra (Fig. 13b) revealed the reduction took place on the surface of GO/PDDA/Fe_3O_4 with the subsidiarity of π electrons carbocyclic six-membered ring [44]. Moreover, differential pulse voltammetry (DPV) with a conventional three-electrode system was also employed to verify the reduction in the presence of GO/PDDA/Fe_3O_4 and GO/PDDA (1.0 mg/mL). The appeared response current (Fig. 13c) was inversely proportional to the pH values, and the differential pulse voltammetry (DPV) (Fig. 13c) at different pH were recorded. The experiment stated the pH could strongly affect the sensitivity and intension of the chromium reduction peak, indicating a better reduction in highly acidic circumstances and a disappearance of the reduction peak at pH = 4.5. Given the above, the schematic representation for the adsorption of Cr(VI) ions by GO/PDDA/Fe_3O_4 is shown as Fig.14.

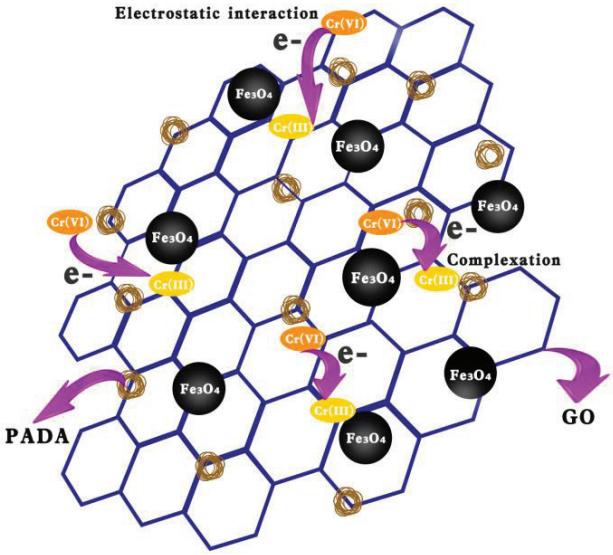

Fig. 14. The schematic representation for adsorption of Cr(VI) by GO/PDDA/Fe_3O_4.

3.6. Filtration-adsorption and filtration-desorption results

Although the decontamination capacity of 141.68 mg/g for GO/PDDA/Fe_3O_4 was not higher than all the reported graphene-based adsorbents in Table 2 [10,21,45–50]. In view of the instantaneous adsorption capacity of GO/PDDA/Fe_3O_4 towards Cr(VI), the GO/PDDA/Fe_3O_4-filled membranes were applied in filtration-adsorption. The concentration of Cr(VI) in the filtered liquid was determined by ICP-AES and the adsorption results are shown in Figs. 15a–c. To give an intuitive display, Fig. 15a shows that the orange faded away immediately after filtration-adsorption, and Fig. 15b also presents the filtration-desorption effect by 0.1 mol/L NaOH + 0.1 mol/L NaCl solution. The explicit removal efficiency of the GO/PDDA/Fe_3O_4-filled membranes towards Cr(VI) solution with different concentrations (10–60 mg/L, 10 mg/L intervals) is displayed in Fig. 15c. Meanwhile, 5 mg and 10 mg synthetized GO/PDDA/Fe_3O_4 filler exhibited removal efficiency of 83.0%~97% and 97.0~98.9%, respectively. These results stated GO/PDDA/

Table 2
Representative reported adsorption studies on the removal of Cr(VI) by graphene-based materials

Adsorbent	Conc. (mg/L)	pH	Temp. (K)	Contact time (min)	q_e (mg/g)	Ref.
CTAB modified graphene	20–100	2	333	60	21.50	[45]
Graphene/Fe	25–125	4	293	240	162	[10]
Graphene/MgAl-layered double hydroxides	50–250	2	–	1440	183.82	[46]
RGO/Fe(0)/Fe_3O_4	2–6	7	298	60	31.1	[47]
GO/chitosan/ferrite nano composite	10–125	2	300	600	270.27	[48]
TEPA/polypyrrole/GO aerogel	100	2	298	300	408.48	[49]
GO/Fe_3O_4 nanoparticles	33	2	318	720	123.4	[50]
Polypyrrol/GO/Fe_3O_4	48–250	3	318	720	293.3	[21]
GO/PDDA/Fe_3O_4	10–60	2	Room Temp.	~0	141.68	This work

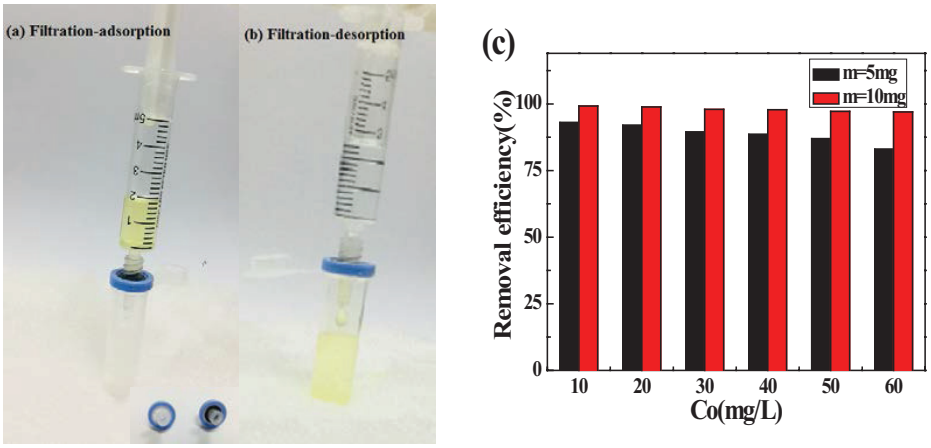

Fig. 15. (a,b) Filtration-adsorption and filtration-desorption comparing demonstration by GO/PDDA/Fe_3O_4-filled membranes; (c) Removal efficiency of filtration-adsorption towards different initial Cr(VI) concentration (pH = 2) by GO/PDDA/Fe_3O_4-filled membranes.

Fe_3O_4 could be regarded as a good candidate for practical filtration-adsorption application.

4. Conclusions

GO/PDDA/Fe_3O_4 magnetic nanocomposites were successfully fabricated by a two-step method. GO was embellished with charged-polymer PDDA and Fe_3O_4, and a relatively high adsorption capacity for Cr(VI) could be achieved. The magnetic separation properties could implement the adsorbent a real-life application. As we all know, the solution pH made a big influence to the Cr(VI) take-in. The experiments indicated the maximum adsorption capacity reached 141.68 mg/g at pH = 2 and the fitting pseudo-second-order model illustrated the process was mostly chemisorption. The desorption-regeneration results showed that the adsorption capacity could remain relatively stable undergoing several times of usage. Through the filling GO/PDDA/Fe_3O_4 into the membranes for filtration-adsorption, satisfactory results including high removal efficiency could be obtained. In conclusion, GO/PDDA/Fe_3O_4 had the prospect to realize effective and economic dispose of Cr(VI) from wastewater, or be used as a filter material for filtration-adsorption.

Acknowledgements

This work was supported by the National Natural Science Foundation of China (No.21571191 and No.51674292), Provincial Natural Science Foundation of Hunan (2016JJ1023), Fundamental Research Funds for the Central Universities of Central South University (2018zzts367), and Key Laboratory of Hunan Province for Water Environment and Agriculture Product Safety (2018TP1003).

References

[1] N.K. Lazaridis, D.N. Bakoyannakis, E.A. Deliyanni, Chromium(VI) sorptive removal from aqueous solutions by nanocrystalline akaganèite, Chemosphere, 58 (2005) 65–73.
[2] Y. Xu, D. Zhao, Reductive immobilization of chromate in water and soil using stabilized iron nanoparticles, Water Res., 41 (2007) 2101–2108.
[3] Y. Lin, W. Cai, X. Tian, X. Liu, G. Wang, C. Liang, Polyacrylonitrile/ferrous chloride composite porous nanofibers and their strong Cr-removal performance, J. Mater. Chem., 21 (2011) 991–997.
[4] D. Petruzzelli, R. Passino, G. Tiravanti, Ion exchange process for chromium removal and recovery from tannery wastes, Water Sci. Technol., 34 (1995) 2612–2617.
[5] J.-K. Yang, S.-M. Lee, Removal of Cr(VI) and humic acid by using TiO_2 photocatalysis, Chemosphere, 63 (2006) 1677–1684.
[6] Y.-X. Liu, D.-X. Yuan, J.-M. Yan, Q.-L. Li, T. Ouyang, Electrochemical removal of chromium from aqueous solutions using electrodes of stainless steel nets coated with single wall carbon nanotubes, J. Hazard. Mater., 186 (2011) 473–480.
[7] X. Feng, C. Liang, J. Yu, X. Jiang, Facile fabrication of graphene oxide-polyethylenimine composite and its application for the Cr(VI) removal, Sep. Sci. Technol., 53 (2018) 2376–2387.
[8] C. Liang, X. Feng, J. Yu, X. Jiang, Facile one-step hydrothermal syntheses of graphene oxide-MnO_2 composite and their application in removing heavy metal ions, Nano-Micro Lett., 13 (2018) 1179–1184.
[9] F. Zhou, X. Feng, J. Yu, X. Jiang, High performance of 3D porous graphene/lignin/sodium alginate composite for adsorption of Cd(II) and Pb(II), Environ, Sci. Pollut. Res., 25 (2018) 15651–15661.
[10] H. Jabeen, V. Chandra, S. Jung, J.W. Lee, K.S. Kim, S.B. Kim, Enhanced Cr(VI) removal using iron nanoparticle decorated graphene, Nanoscale, 3 (2011) 3583–3585.
[11] S. Chowdhury, R. Balasubramanian, Recent advances in the use of graphene-family nanoadsorbents for removal of toxic pollutants from wastewater, Adv. Colloid Interface Sci., 204 (2014) 35–56.
[12] S. Zhang, M. Zeng, W. Xu, J. Li, J. Li, J. Xu, X. Wang, Polyaniline nanorods dotted on graphene oxide nanosheets as a novel super adsorbent for Cr(VI), Dalton Trans., 42 (2013) 7854–7858.
[13] H. Ge, Z. Ma, Microwave preparation of triethylenetetramine modified graphene oxide/chitosan composite for adsorption of Cr(VI), Carbohydr. Polym., 131 (2015) 280–287.
[14] P.K. Kanaujia, D. Pardasani, A.K. Purohit, V. Tak, D.K. Dubey, Polyelectrolyte functionalized multi-walled carbon nanotubes as strong anion-exchange material for the extraction of acidic degradation products of nerve agents, J. Chromatogr. A, 1218 (2011) 9307–9313.
[15] B.P. Tripathi, N.C. Dubey, M. Stamm, Functional polyelectrolyte multilayer membranes for water purification applications, J. Hazard. Mater., 252–253 (2013) 401–412.

[16] X. Wang, Z. Liu, X. Ye, K. Hu, H. Zhong, J. Yu, M. Jin, Z. Guo, A facile one-step approach to functionalized graphene oxide-based hydrogels used as effective adsorbents toward anionic dyes, Appl. Surf. Sci., 308 (2014) 82–90.
[17] W. Ren, Y. Fang, E. Wang, A binary functional substrate for enrichment and ultrasensitive SERS spectroscopic detection of folic acid using graphene oxide/Ag nanoparticle hybrids, ACS Nano, 5 (2011) 6425–6433.
[18] J. Hu, I.M.C. Lo, G. Chen, Comparative study of various magnetic nanoparticles for Cr(VI) removal, Sep. Purif. Technol., 56 (2007) 249–256.
[19] L.C. Oliveira, R.V.R. Rios, J.D. Fabris, K. Sapag, V.K. Garg, R.M. Lago, Clay-iron oxide magnetic composites for the adsorption of contaminants in water, Carbon, 22 (2003) 169–177.
[20] M. Liu, T. Wen, X. Wu, C. Chen, J. Hu, J. Li, X. Wang, Synthesis of porous Fe_3O_4 hollow microspheres/graphene oxide composite for Cr(VI) removal, Dalton Trans., 42 (2013) 14710–14717.
[21] H. Wang, X. Yuan, Y. Wu, X. Chen, L. Leng, H. Wang, H. Li, G. Zeng, Facile synthesis of polypyrrole decorated reduced graphene oxide-Fe_3O_4 magnetic composites and its application for the Cr(VI) removal, Chem. Eng. J., 262 (2015) 597–606.
[22] T. Wang, L. Zhang, C. Li, W. Yang, T. Song, C. Tang, Y. Meng, S. Dai, H. Wang, L. Chai, J. Luo, Synthesis of core-shell magnetic Fe_3O_4@poly(m-phenylenediamine) particles for chromium reduction and adsorption, Environ. Sci. Technol., 49 (2015) 5654–5662.
[23] G. Wójcik, Z. Hubicki, Sorption and reduction of chromate(VI) ions on Purolite A 830, Sep. Sci. Technol., 51 (2016) 2539–2546.
[24] G. Wójcik, Z. Hubicki, Investigations of chromium (VI) ion sorption and reduction on strongly basic anion exchanger, Sep. Sci. Technol., 53 (2017) 1088–1096.
[25] Y.S. Ho, G. Mckay, Pseudo-second order model for sorption processes, Process Biochem., 34 (1999) 451–465.
[26] W.J. Weber, J.C. Morris, Kinetics of adsorption on carbon from solution, J. Sanit. Eng. Div. Am. Soc. Civ. Eng., 89 (1963) 31–60.
[27] J. Yang, X. Jiang, F. Jiao, J. Yu, The oxygen-rich pentaerythritol modified multi-walled carbon nanotube as an efficient adsorbent for aqueous removal of alizarin yellow R and alizarin red S, Appl. Surf. Sci., 436 (2018) 198–206.
[28] X. Xu, J. Zou, J. Teng, Q. Liu, X. Jiang, F. Jiao, J. Yu, X. Chen, Novel high-gluten flour physically cross-linked graphene oxide composites: Hydrothermal fabrication and adsorption properties for rare earth ions, Ecotoxicol. Environ. Saf., 166 (2018) 1–10.
[29] R.D. Martínez-Orozco, H.C. Rosu, S.-W. Lee, V. Rodríguez-González, Understanding the adsorptive and photoactivity properties of Ag-graphene oxide nanocomposites, J. Hazard. Mater., 263 (2013) 52–60.
[30] M. Anbia, S. Salehi, Synthesis of polyelectrolyte-modified ordered nanoporous carbon for removal of aromatic organic acids from purified terephthalic acid wastewater, Chem. Eng. Res. Des., 90 (2012) 975–983.
[31] A. Misra, P.K. Tyagi, M.K. Singh, D.S. Misra, FTIR studies of nitrogen doped carbon nanotubes, Diamond Relat. Mater., 15 (2006) 385–388.
[32] A.L.M. Reddy, A. Srivastava, S.R. Gowda, H. Gullapalli, M. Dubey, P.M. Ajayan, Synthesis of nitrogen-doped graphene films for lithium battery application, ACS Nano, 4 (2010) 6337–6342.
[33] X. Xu, X. Jiang, F. Jiao, X. Chen, J. Yu, Tunable assembly of porous three-dimensional graphene oxide-corn zein composites with strong mechanical properties for adsorption of rare earth elements, J. Taiwan Inst. Chem. Eng., 85 (2018) 106–114.
[34] J. Zou, L. Huang, X. Jiang, F. Jiao, J. Yu, Electrochemical behaviors and determination of rifampicin on graphene nanoplatelets modified glassy carbon electrode in sulfuric acid solution, Desal. Wat. Treat., 120 (2018) 272–281.
[35] B. Yue, L. Yu, F. Jiao, X. Jiang, J. Yu, The fabrication of pentaerythritol pillared graphene oxide composite and its adsorption performance towards metal ions from aqueous solutions, Desal. Wat. Treat., 102 (2018) 124–133.
[36] H.-P. Cong, X.-C. Ren, P. Wang, S.-H. Yu, Macroscopic multifunctional graphene-based hydrogels and aerogels by a metal ion induced self-assembly process, ACS Nano, 6 (2012) 2693–2703.
[37] M. Bhaumik, A. Maity, V.V. Srinivasu, M.S. Onyango, Enhanced removal of Cr(VI) from aqueous solution using polypyrrole/Fe_3O_4 magnetic nanocomposite, J. Hazard. Mater., 190 (2011) 381–390.
[38] J. Hu, G. Chen, I.M.C. Lo, Removal and recovery of Cr(VI) from wastewater by maghemite nanoparticles, Water Res., 39 (2005) 4528–4536.
[39] A. Shahbazi, H. Younesi, A. Badiei, Functionalized SBA-15 mesoporous silica by melamine-based dendrimer amines for adsorptive characteristics of Pb(II), Cu(II) and Cd(II) heavy metal ions in batch and fixed bed column, Chem. Eng. J., 168 (2011) 505–518.
[40] G. Zeng, Y. Pang, Z. Zeng, L. Tang, Y. Zhang, Y. Liu, J. Zhang, X. Lei, Z. Li, Y. Xiong, G. Xie, Removal and recovery of Zn^{2+} and Pb^{2+} by imine-functionalized magnetic nanoparticles with tunable selectivity, Langmuir, 28 (2012) 468–473.
[41] L. Wang, J. Zhang, R. Zhao, C. Li, Y. Li, C. Zhang, Adsorption of basic dyes on activated carbon prepared from polygonum orientale linn: equilibrium, kinetic and thermodynamic studies, Desalination, 254 (2010) 68–74.
[42] S. Chen, Q. Yue, B. Gao, X. Xu, Equilibrium and kinetic adsorption study of the adsorptive removal of Cr(VI) using modified wheat residue, J. Colloid Interface Sci., 349 (2010) 256–264.
[43] S. Deng, R. Bai, Adsorption and desorption of humic acid on aminated polyacrylonitrile fibers, J. Colloid Interface Sci., 280 (2004) 36–43.
[44] Y. Zhang, H.-L. Ma, J. Peng, M. Zhai, Z.-Z. Yu, Cr(VI) removal from aqueous solution using chemically reduced and functionalized graphene oxide, J. Mater. Sci., 48 (2013) 1883–1889.
[45] Y. Wu, H. Luo, H. Wang, C. Wang, J. Zhang, Z. Zhang, Adsorption of hexavalent chromium from aqueous solutions by graphene modified with cetyltrimethylammonium bromide, J. Colloid Interface Sci., 394 (2013) 183–191.
[46] X. Yuan, Y. Wang, J. Wang, C. Zhou, Q. Tang, X. Rao, Calcined graphene/MgAl-layered double hydroxides for enhanced Cr(VI) removal, Chem. Eng. J., 221 (2013) 204–213.
[47] P. Bhunia, G. Kim, C. Baik, H. Lee, A strategically designed porous iron-iron oxide matrix on graphene for heavy metal adsorption, Chem. Commu., 48 (2012) 9888–9890.
[48] M.S. Samuel, S.S. Shah, V. Subramaniyan, T. Qureshi, J. Bhattacharya, N.D. Pradeep Singh, Preparation of graphene oxide/chitosan/ferrite nanocomposite for chromium(VI) removal from aqueous solution, Int. J. Biol. Macromol, 119 (2018) 540–547.
[49] Q. Liang, H. Luo, J. Geng, J. Chen, Facile one-pot preparation of nitrogen-doped ultra-light graphene oxide aerogel and its prominent adsorption performance of Cr(VI), Chem. Eng. J., 338 (2018) 62–71.
[50] D. Zhao, X. Gao, C. Wu, R. Xie, S. Feng, C. Chen, Facile preparation of amino functionalized graphene oxide decorated with Fe_3O_4 nanoparticles for the adsorption of Cr(VI), Appl. Surf. Sci., 384 (2016) 1–9.